Atomic-Scale Insights into the High Dielectric Permittivity of Bismuth Silicate Glass

J. R. Stellhorn

Co-Creation Institute for Advanced Materials,
Shimane University, Shimane 690-8504,
Japan & Department of Material Chemistry,
Graduate School of Engineering, Kyoto University, Kyoto 615-8520, Japan *

A. Masuno

Department of Material Chemistry, Graduate School of Engineering,
Kyoto University, Kyoto 615-8520, Japan

Y. Onodera and S. Kohara

Center for Basic Research on Materials,
National Institute for Materials Science, Tsukuba, Ibaraki 305-0047, Japan

K. Yoshida

Graduate school of Science and Technology,
Hirosaki University, Aomori 036-8561, Japan

Y. Yanaba and H. Inoue

Institute of Industrial Science, The University of Tokyo, Tokyo 153-8505, Japan

T. Ohkubo

Graduate School of Engineering, Chiba University, Chiba 263-8522, Japan

H. Taniguchi

Department of Physics, Nagoya University,
Furo-cho, Nagoya 464-8602, Japan

(Dated: September 27, 2025)

Abstract

The amorphous phase of bismuth silicate (Bi_2SiO_5) is characterized by an exceptionally large dielectric permittivity over a wide temperature range. This study explores the relationship between this remarkable property and the material's atomic-scale structure, which has been modeled from experimental X-ray and neutron scattering as well as EXAFS and NMR spectroscopy data in a Reverse Monte-Carlo approach. The resulting structural model is analyzed to reveal short- and intermediate-range features on the atomic scale.

Our results show that the exceptional dielectric performance stems from the asymmetric coordination of Bi-O_x polyhedra as well as a nano-segregation induced by SiO_4 chains, which together boost local polarizability. These findings establish a direct link between disordered atomic structures and enhanced dielectric properties, and sets a new benchmark for amorphous materials.

I. INTRODUCTION

Amorphous compounds and glasses are not typically associated with high a dielectric permittivity. Notable applications in this area, for instance as capacitor materials, are therefore largely limited to some specialized devices that demand extremely high stability, reliability, and/or tolerance to high voltages and temperatures. In this article, we report on a bismuth silicate glass that possesses a high dielectric permittivity and a low dielectric loss over a wide temperature range from 200 to 600 K. Such properties make it a promising candidate for more widespread applications.

The dielectric permittivity, usually denoted by the dielectric constant ε, is a dimensionless property that quantifies a material's ability to store electrical energy in response to an applied electric field. In crystalline materials, a high permittivity is often achieved through collective atomic displacements or long-range polar order, whereas in glasses such mechanisms are generally suppressed by structural disorder. The vast majority of known amorphous materials therefore exhibit values of ε lower than 12. Adding heavier elements, in particular Ba or Pb, can increase this value to around 20 [1–3], or even 30 with further addition of Bi [4, 5]. An suitable overview of the distribution glasses taken from the SciGlass Next database [6] with reported ε values is given in Figure 1 A. The newly investigated bis-

* jrstellhorn@mat.shimane-u.ac.jp

muth silicate glass phase, a-Bi_2SiO_5 (or a-BSO), prominently stands out, reaching a value of 56. For comparison, this value is even larger then the reported value for crystalline bismuth oxide (Bi_2O_3, with $\varepsilon \approx 33$[7]) and just short of that of crystalline bismuth silicate (Bi_2SiO_5, with $\varepsilon \approx 90$ [8]). The latter is a wide-gap semiconductor, with a reported band gap of about 3.8 eV [8]. Both c-Bi_2O_3 and c-Bi_2SiO_5 contain Bi in the nominal 3+ valence state, where the presence of a stereochemically active lone pair gives rise to a large inherent polarizability [9, 10].

We measured the dielectric response of the Bi_2SiO_5 glass in temperature range between 200 and 600 K (Figure 1 B). In this wide temperature region, ε varies only in a narrow region between 54 and 64. The dielectric loss is small in the range up to about 500 K with a value of about 0.5%, but starts to increase above that temperature. Note that the material itself is stable until about 750 K before it starts to crystallize.

Further exceptional optical properties of bismuth oxide-based glasses have been reported in various reviews, such as a high linear refractive index, low glass transition temperature, and a high third-order nonlinear optical susceptibility[10, 11]. Additionally, their large electronic polarizability has been characterized using the concepts of optical basicity and the interionic interaction parameter [10]. It was found that Bi_2O_3-based glasses exhibit an distinctly strong basic nature and weak chemical bond strength among the various oxide glasses. These properties are attributed to the high cation polarizability of Bi^{3+} and the presence of an electron lone pair in the valence shell [9].

While the dielectric properties of crystalline materials, and their relationship with the atomic structure, have been extensively studied, amorphous compounds present a distinctive challenge due to their structural disorder and lack of long-range order. Understanding and characterizing their dielectric behavior is essential both for fundamental scientific exploration as well as for uncovering novel technological applications.

One of the few notable examples in which the intricate correlation between the atomic structure of an amorphous compound and their optical properties has been thoroughly investigated are chalcogenide glasses for their application as phase-change materials. In these systems, the dielectric permittivity is closely tied to intermediate-range atomic order: the theoretical framework described by Huang and Robertson [12] presents a link between the optical properties of Ge-Te glasses and angular order at the second-neighbor level , which plays a crucial role in aligning bond orbitals. This alignment can facilitate the formation

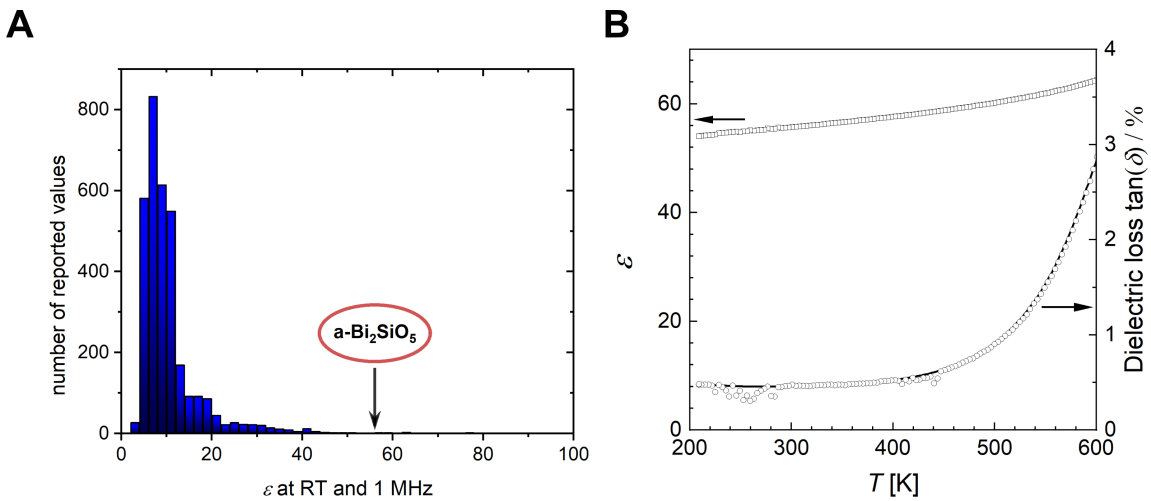

FIG. 1. (**A**) Histogram of all tabulated values of dielectric constants ε (at 1 MHz and room temperature) in the SciGlassNext database [6]. (**B**) Measurement of the dielectric properties, relative permittivity ε and dielectric loss function $\tan(\delta)$, of Bi_2SiO_5 glass as a function of temperature.

of 'resonant' [13] bonding configurations. In contrast, the absence of resonant bonding in the crystalline phase of Cu_2GeTe_3 (a novel phase-change material), where tetrahedral coordination dominates, leads to the unusual scenario where the amorphous phase exhibits a higher dielectric permittivity than the crystal. This phenomenon results in a negative optical contrast between the crystalline and amorphous phase [14, 15]. Even though the exact mechanism is likely to be different in oxide glasses, such findings emphasize the importance to look beyond the atomic short-range order to understand the optical properties of glasses.

The corresponding crystal structure of Bi_2SiO_5 (c-BSO) in itself has been a subject of extensive research, especially with regard to its dielectric properties. The c-BSO structure consists of one-dimensional chains of SiO_4 tetrahedra running along the c axis, which are sandwiched by a double layer of BiO_6 polyhedra [8, 16]. This stoichiometric crystal structure exists only in the non-equilibrium phase diagram; it can be fabricated from a crystallization of the glass. In this process, the system initially crystallizes at about 470 °C into a phase that contains crystalline bismuth oxide (c-Bi_2O_3) and amorphous silica (a-SiO_2), from which the c-BSO phase is formed at about 540-600 °C [8, 16]. Furthermore, dielectric measurements of c-BSO have demonstrated that its ferroelectricity disappears in association with disordering of the SiO_4 chains through La doping, highlighting the critical role of these chains in the material's ferroelectric behavior [16].

Other comparable crystalline phases with a nominal Bi^{3+} state, like c-Bi_2O_3, also consist of interconnected BiO_5 or BiO_6 polyhedra. The geometry of these polyhedra is determined by the Bi lone pair, resulting in an asymmetrical bonding configuration in which all oxygen atoms are basically constrained to one hemisphere around Bi. The opposite side is occupied by the electron lone pair. This arrangement leads to substantial atomic-level polarizability, contributing to the large dielectric constant observed in the crystal phase.

Previous structural characterizations of the amorphous phase of the Bi_2O_3-SiO_2 system are reported by Witkowska et al. [17], and for low contents of Bi_2O_3 by Ohkura et al. [18]. However, these works are mainly based on X-ray Absorption Fine Structure spectroscopy (XAFS), and do not propose a detailed structural model, since this method typically probes only the immediate short-range order. In these glasses, the XAFS investigations observe only the nearest O atoms around Bi [17, 18], with a reported coordination number of 3.0 at a bond distance of 2.26 Å for the Bi_2SiO_5 glass [17]. Beyond the short-range order, an investigation by ^{29}Si Magic-Angle Spinning Nuclear Magnetic Resonance (MAS-NMR) spectroscopy by Todea et al. [19] confirmed that most SiO_4 units are part of chain structures. Infrared and Raman spectroscopy data [20] further indicate that Bi maintains a 3+ valence state in amorphous Bi-O systems, analogous to the crystalline phases. This suggests the persistence of a stereochemically active lone pair, which would provide a natural link between local structure and the pronounced dielectric properties of a-BSO. However, the much greater configurational freedom to arrange Bi-O units in the amorphous state makes it highly challenging to determine the actual local geometry.

Our new study on a-BSO is based on a more comprehensive experimental approach. We thereby establish a reliable model of the atomic structure, and shed light on the origin of the materials' distinct physical properties. In addition, we compare the local atomic geometry of the amorphous phase with that of the crystal, in order to assess how the larger configurational freedom of Bi-O units influences the material's dielectric response.

II. EXPERIMENT AND ANALYSIS

a. Sample preparation To prepare the Bi_2SiO_5 glass samples, first Bi_2O_3 and SiO_2 powders were mixed in equimolar portions and sintered at 800 °C for 12 h. Then, small beads of amorphous samples were synthesized by rapid quenching of the laser-heated melts using a containerless aerodynamic levitation technique [21].

b. Composition analysis The composition of the sample was checked by Inductively Coupled Plasma Optical Emission Spectroscopy (ICP-OES). We found the following ratios of Bi and Si: Bi 79.0 wt.%, Si 5.60 wt.%. This indicates that a small amount of Bi_2O_3 is evaporated during the sample preparation, and the actual composition is $Bi_{1.9}SiO_{4.84}$. However, for simplicity, we still refer to the nominal composition in the main text.

c. Optical transmittance measurements We performed optical transmittance measurements of the Bi_2SiO_5 glass. From these, we can estimate that the optical band-gap energy is 3.0 eV. For reference, crystalline BSO was reported to have a bandgap of approximately 3.8 eV[22]. Note that the bandgap of glasses is generally smaller than that of comparable crystals because of their amorphous nature.

d. Scattering experiments Total X-ray scattering experiments were performed at SPring-8 beamline BL04B2 at an energy of 113 keV. The weighting factors for the partial S(Q)'s in X-ray scattering depend on the scattering vector. Approximate values at the structure factor maximum (Q=2 Å^{-1}) are 0.60, 0.09, 0.26, 0.003, 0.02 and 0.03 for the Bi-Bi, Bi-Si, Bi-O, Si-Si, Si-O and O-O correlations, respectively.

Additionally, neutron scattering experiments were performed at the high intensity total diffractometer NOVA, installed at BL21 of the Materials and Life Science (MLF) Experimental Facility at the J-PARC spallation neutron source, with a reciprocal space range of up to 30 Å^{-1}. The weighting factors depend on the scattering length of the atomic core, and are 0.1154, 0.0562, 0.3925, 0.0068, 0.0954 and 0.3337 (same order as above).

e. EXAFS experiments Extended X-ray absorption spectroscopy experiments at the Bi L_3 edge were performed at the KEK-PF beamline BL27B in transmission mode. The near-edge region of both crystalline and amorphous Bi_2SiO_5 coincides well, and there is no observable shift between them, indicating that both systems share a similar electronic state of Bi^{3+}.

f. ^{29}Si MAS NMR The ^{29}Si MAS NMR spectroscopy measurements were performed on a JEOL JNM-ECA 500 spectrometer equipped with a MAS probe head (zirconia rotor with 4 mm diameter) at 11.74 T (500 MHz). The ^{29}Si NMR spectra were recorded using $\pi/6$ pulses (1.5 μs) at a spinning rate of 10 kHz, a relaxation delay of 1 s, and 50,000 accumulated signal transients. The ^{29}Si chemical shift was referenced to an external standard, sodium 3-(trimethylsilyl) propionate 2.2.3.3-d4 (+1.445 ppm).

From the ^{29}Si MAS NMR data, the ratios Q^n of the connection between SiO_4 tetrahedra can be extracted (where n is the number of bridging oxygen). The result is about 90% for Q^2 species, i.e. corner-sharing tetrahedra arranged in a 1-D chain, and 10% for Q^3 species, i.e. forming a 2-D network of corner-sharing tetrahedra. This information was included in the RMC modeling procedure.

g. Measurement of dielectric constants Dielectric measurements were performed in a temperature range from 200 to 600 K using a lab-made system equipped with a precision LCR meter Keysight E4980A and a temperature controller Linkam THMS600.

h. RMC analysis We employed the RMC_POT package for the Reverse Monte Carlo (RMC) modeling [23, 24], with a box containing 2455 Bi, 1292 Si and 6253 O atoms (corresponding to the actual composition) in the appropriate density (0.06685 atoms/Å^3). Nearest neighbor distances were defined as (in Å) 3.3, 3.3, 2.0, 3.1, 1.4 and 2.5 for the Bi-Bi, Bi-Si, Bi-O, Si-Si, Si-O and O-O pairs, respectively. Furthermore, constraints on the Si-O correlation were included to realize an environment in which every Si is surrounded by exactly 4 O neighbors in a tetrahedral coordination, and to suffice the second-nearest neighbor constraints that were determined experimentally from the ^{29}Si NMR, with $Q^2 = 90\%$ and $Q^3 = 10\%$ of all SiO_4 units. This coordination geometry was retained during the entire modeling procedure by fixed neighbor constraints (FNC) and second-neighbor constraints, respectively. An additional coordination constraint was placed on Bi atoms to exclude extremely under-coordinated cases, i.e. Bi-O coordination numbers of 0, 1 and 2.

The experimental data from X-ray and neutron scattering, as well as the Bi L_3 edge EXAFS data were used as input. Additionally, the Fourier transform of the neutron structure factor was used to improve the shape of the pair correlation functions in the range below 5.4 Å. For the EXAFS data, a fit of the energy shift value ΔE_0 was allowed, and determined to be 2.3 eV. The starting configuration consisted of SiO_4 units with appropriate Q^n connections, while Bi and the remaining O atoms were added at random positions. The final RMC fit qualities were determined with $R_{\mathrm{neutron\,g(r)}} = 0.037$, $R_{\mathrm{neutron\,S(Q)}} = 0.061$, $R_{\mathrm{X-ray\,S(Q)}} = 0.073$ and $R_{\mathrm{EXAFS\,\chi(k)}} = 0.259$.

i. Persistence Homology For the Persistence Homology (PH) analysis, the HomCloud package was used [25]. The PH analysis offers a possibility to extract multi-scale information about topological features of an atomic configuration. The homology is expressed as a 2D histogram called persistence diagram (PD) [26–29], typically illustrated with a 'birth' and 'death' coordinate of a feature of interest. For the input configuration, we used the RMC-derived model with 10,000 atoms of a-BSO, and compare it with supercells of the crystal phases of BSO and Bi_2O_3 containing a comparable amount of atoms.

This approach allows for an extended view into the intermediate-range order of a system. More detailed descriptions of this method can be found in the indicated references, along with examples for Cu-Zr [27] and SiO_2 [28] glasses.

j. Cluster analysis The 'cluster approach' considers the immediate environment around a specific element. In this approach, the nearest neighbors around each atom of the same element (Si and Bi respectively, in our case) are determined within a certain cut-off distance, which was set to 2.0 Å for Si and 2.85 Å for Bi, respectively, according to the extent of the first coordination shell from the partial pair distribution functions. Then, this cluster is isolated from the rest of the configuration. Its geometric center, i.e. the center of gravity of the oxygen atoms, is then translated to the origin of the coordinate system. The shift of the central atom from the origin then includes some information on the symmetry of the cluster: in a symmetric case, e.g. a regular SiO_4 tetrahedron, the Si atom will be located at the center of gravity, but any distortion will shift it away from this position.

Using the same clusters, another analysis can be performed: determining the central atom's chemical bonds' spherical harmonics parameters. The concept of using spherical harmonics (SH) parameters is an established approach to characterize bond-orientational order in liquids and glasses [30, 31]. They can be considered as quantitative descriptors of the angular distribution of interatomic vectors [32–34]. We denote the SH functions as $Y_{l,m}$ with order l and degree m for the angular coordinates.

The sum the of spherical harmonics is represented by the coefficient $q_{l,m}$:

$$q_{l,m} = \frac{1}{N} \sum_{i}^{N} Y_{l,m}^{i} \tag{1}$$

Averaging over all allowed values m for a given index l leads to a quantitative descriptor that is independent of any set of reference axes:

$$q_l = \sqrt{\frac{4\pi}{2l+1}\left(\sum_{m=-l}^{l} q_{l,m}\right)^2} \quad (2)$$

In the structure analysis using these rotationally invariant descriptors q_l, higher-symmetry arrangements (e.g. cubic, tetrahedral) exhibit a higher degree of variability than lower symmetry environments (e.g. triangular or random)[32], so that the variance of q_l can be used as a quantitative descriptor of local symmetry.

While the reference crystal structures possess a limited number of unique q_l values for each atomic site, the atomic configuration obtained from RMC modeling comprises one value for each central atom, and necessitates a statistical analysis.

III. RESULTS

As outlined in the Experimental section, we use a combination of several experimental characterizations (X-ray and neutron scattering, Bi XAFS, Si MAS NMR) integrated in a Reverse Monte Carlo modeling approach to extract information on the atomic-scale structure of amorphous bismuth silicate.

One of our main research objectives is to clarify whether the atomic structural information allows to draw conclusions regarding the exceptionally large dielectric permittivity of a-Bi_2SiO_5. The corresponding geometries in Bi-O crystal phases represent suitable starting points for further considerations. They indicate that the free electron pair at Bi, and the asymmetrical bonding configuration connected with it, is one of the most important factors leading to a significant polarizability. One major piece of this puzzle is therefore to analyze if similar local environments can be identified in the amorphous phase on the short-range order (SRO) scale. Furthermore, as noted in the introduction, there can be a significant discrepancy in the dielectric permittivity even for similar local building blocks, as is the case in c-Bi_2SiO_5 vs. c-Bi_2O_3. Their main difference lies in the atomic intermediate-range order (IRO) - i.e. the separation of the BiO_6 double layers in c-BSO. Therefore, it stands to reason that a characterization of the IRO of the amorphous phase may also provide further helpful information.

Moreover, we also aim to elucidate why this material follows a 2-step crystallization process (from a-BSO via a Bi_2O_3 phase to c-BSO), instead of a direct transformation (from a-BSO to c-BSO). Understanding this pathway is crucial for elucidating the crystallization kinetics, which play a vital role in controlling grain size, phase composition, and defect density, thereby enabling the optimization of the material for advanced device applications.

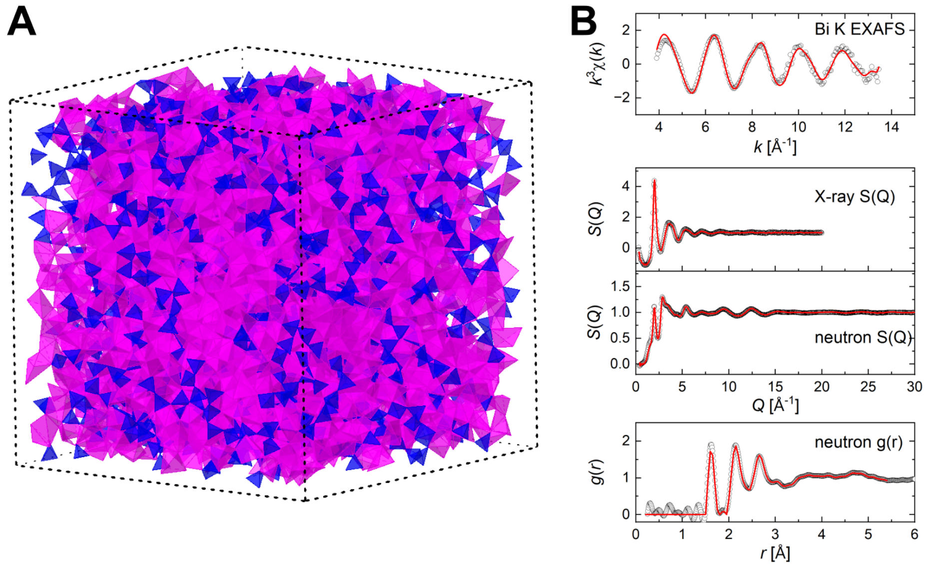

FIG. 2. (**A**) Final configuration of the RMC model with SiO_4 tetrahedra shown in blue and BiO_x ($x = 3 - 7$) polyhedra in purple. (**B**) Fits (red lines) to the experimental data (circles). .

The initial configuration at the start of the modeling procedure consists of appropriately connected SiO_4 units in a box, with the remaining Bi and O atoms placed randomly. From this initial guess, the RMC algorithm optimizes a structure that simultaneously satisfies all available experimental information. The resulting configuration from RMC modeling is displayed in Figure 2 A. In the modeling procedure, the tetrahedral coordination of the SiO_4 units and their connectivity (predominantly Q^2) is constrained, and it is therefore well recognizable in the configuration. The fit results to the experimental data are shown in Figure 2 B.

Looking at the SRO, we first analyze the partial pair correlation functions from the RMC model, as illustrated in Figure 3 A along with running values of the coordination numbers (red lines). All distributions are, naturally, more disordered compared to the crystal phase, however there are several remarkable similarities in the overall short-range order. Notably, the coordination numbers around Bi are 5.3 O atoms (in c-BSO: 6) in the range up to 3.0 Å, 2.4 Si (cryst.: 2), and about 6.5 Bi (cryst.: 6) atoms, all depending on the exact cut-off

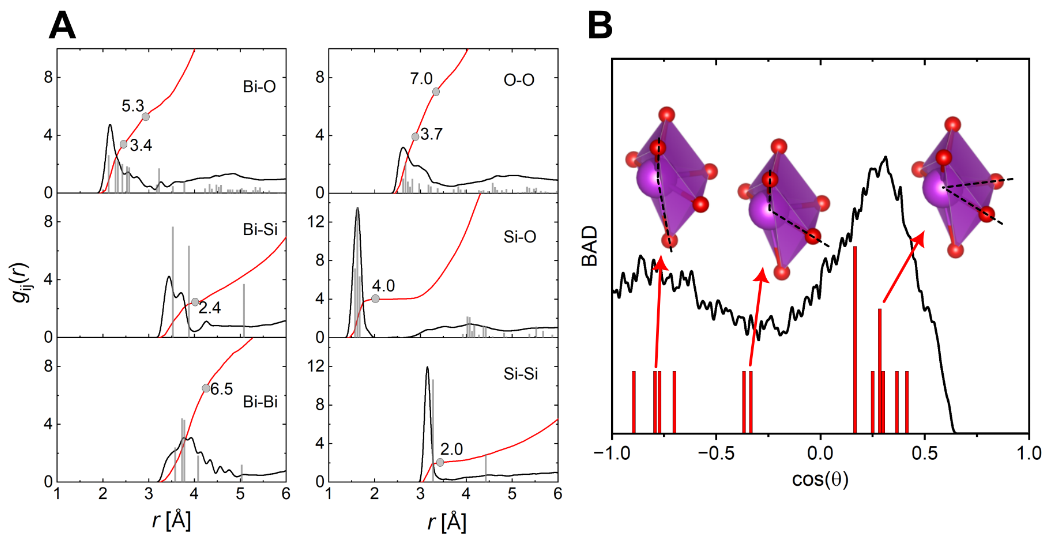

FIG. 3. (**A**) Partial pair correlation functions (black) along with running coordination numbers (red) of the final model, together with a comparison of c-BSO (gray bars). (**B**) The bond angle distributions O-Bi-O obtained from the RMC model (lines) in comparison with the Bi_2SiO_5 crystal structure (bars).

value for the coordination number.

These parameters already hint at the existence (and prevalence) of BiO_5 and BiO_6 clusters. However, they do not yet provide evidence that their local geometry is indeed similar to the crystal - for instance, it is entirely possible that the oxygen atoms could be distributed in a random and/or symmetrical manner around Bi.

A further look into the SRO around Bi can be extracted from the bond angle distributions (BAD) of O around Bi, as shown in Figure 3 B (with a comparison of the BAD of c-BSO). The crystalline BiO_6 polyhedron has 3 main regions of O-Bi-O angles: a relatively wide distribution of around $cos(\theta) \approx 0.3$ (70°), a narrow region around -0.4 (110°), and a wider region again around -0.8 (140°) that is characteristic of the two O atoms facing the empty bond hemisphere. The RMC-derived BAD is naturally broad as a result of both the nature of the amorphous phase and the characteristics of the RMC technique, which tends to prefer more disordered configurations. However, it exhibits maxima in similar regions, with the most pronounced signal centered at 0.28 (73.7°) and a another broad feature around -0.81 (144.1°).

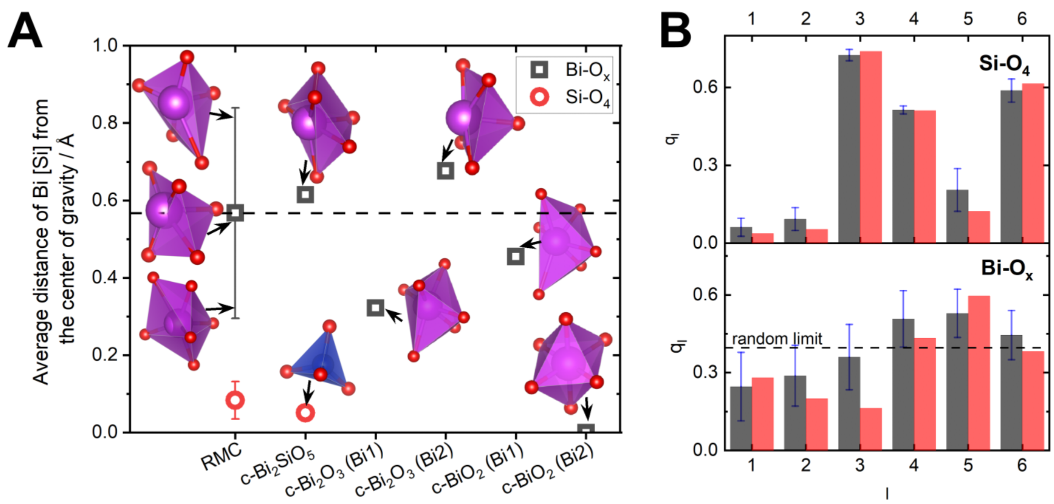

FIG. 4. Analysis of local cluster geometries. (**A**) Shift of Bi [Si] from the cluster centroid in the BiO_x (black squares) and SiO_4 (red circles) clusters, and reference values for comparable crystalline phases. The dashed line is a guide for the eye and set at the average value of the RMC result of BiO_x. Also illustrated are some exemplary model structures (**B**) Analysis of the distribution of bond spherical harmonics parameters for the BiO_x [SiO_4] clusters, comparing the RMC result (black) with c-BSO (red). The dashed line indicates the distribution for a theoretical completely random case. In both cases, the graphs also show the standard deviations of the RMC model.

For investigating the exact distribution of O around Bi, we analyze the local cluster geometries (see e.g. [32–34]) in the RMC model: For each BiO_x ($x \geq 3$) and SiO_4 cluster in the model, the displacement $r_{G,i}$ of the central atom i from the cluster centroid (G) is calculated, as illustrated in Figure 4 A. This distance provides a benchmark for the cluster symmetry, since in a perfectly symmetric cluster $r_{G,i} = 0$. For instance, the SiO_4 units even in c-BSO are not perfectly tetrahedral, but slightly distorted, amounting to a small value of $r_{G,\mathrm{Si}}$ of 0.05 Å. In a similar manner, the SiO_4 units in the RMC model are also sightly distorted by a value of 0.08 Å on average, with a standard deviation of 0.05 Å.

The displacement of Bi from the centroid of the BiO_x clusters is $r_{G,\mathrm{Bi}} = 0.57$ with a standard deviation of 0.27 Å. The large standard deviation is owing to the fact that the RMC procedure generates a wide range of possible local geometries. Exemplary configurations for the smallest and largest deviations are also illustrated in Fig. 4 A. The average value is remarkably close to that found in c-BSO of 0.61 Å. For further comparison, Figure 4 A also shows the displacements in two other bismuth oxides, c-Bi_2O_3 and c-BiO_2. Both include two different types of BiO_x clusters, as illustrated in the toy models in the figure. c-Bi_2O_3 exhibits two local geometries, the first with a smaller displacement (0.32 Å), but the other cluster with an even larger displacement ($r_{G,\mathrm{Bi}} = 0.68$ Å) than c-BSO. We can explain the wide distribution in the RMC model by a continuous mix of such local geometries. On the other hand, more symmetrical distributions around Bi, as in the case of c-BiO_2 with an octahedral geometry ($r_{G,\mathrm{Bi}} = 0.0$ Å), can clearly be ruled out in a-BSO.

Further details on the local symmetry of these clusters can be extracted from an analysis of the bond spherical harmonics (SH) parameters q_l [32, 33] (see 'Methods' section for details). They are displayed in Figure 4 B, again for BiO_x as well as SiO_4 clusters. By design of the RMC model, the statistics of the q_l parameters for the SiO_4 clusters closely match those of the crystalline phase (shown in red). The standard deviations in each value correspond to the variability in the Si-O bond of the RMC model. Both the crystal and amorphous distribution exhibit a large variance of the values: ($var(q_l)$ is 0.06 and 0.08 for a- and c-BSO, respectively). A large variance indicates a high symmetry of the cluster [32], and is a sign of the tetrahedral geometry.

A lower symmetry (= smaller variance) is found in the case of the BiO_x clusters. Note that a theoretical limit for a completely disordered geometry would consist in every value of q_l being equal, as indicated by the dashed line (which is just the average of all q_l). The distribution in a-BSO roughly follows that of c-BSO, with relatively high values at $l = 1, 2$, signifying the polar nature of the cluster. Both exhibit much smaller variances than the SiO_4 units, with $var(q_l)$=0.01 for the amorphous and 0.02 for the crystalline phase. The SH parameters of a-BSO therefore are in line with a cluster symmetry similar to that found in c-BSO, though with a more disordered arrangement.

To characterize the IRO, we employ an analysis of the persistent homology (PH) of the RMC configuration. The PH analysis offers the possibility to extract multi-scale information about topological features. The homology is expressed as a 2D histogram called persistence diagram (PD) [26–29]. These diagrams pick up specific shapes in the data for multiple length scales and for various dimensionalities D_n, e.g. one-dimensional linkages such as ring structures (D_1) or void regions (D_2). The PD's encode certain characteristics of such shapes, in particular the maximum distance between two adjacent atoms in a closed loop and the

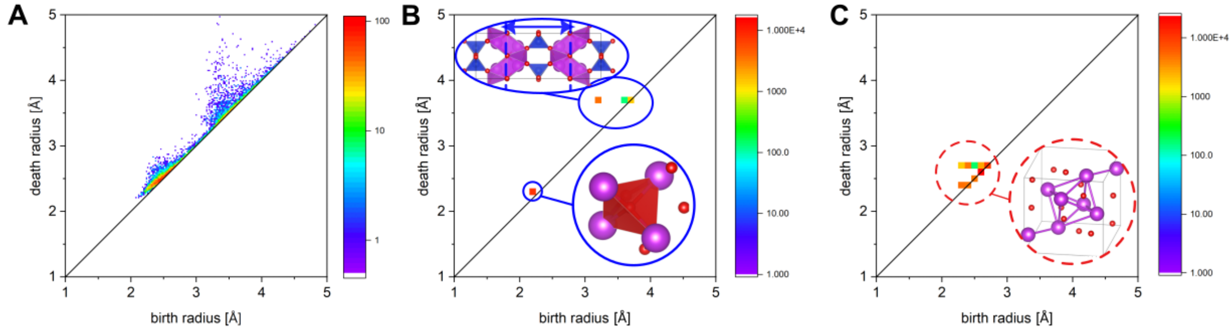

FIG. 5. (**A**) Bi-centric persistence diagrams D_2 from the RMC configuration of a-BSO, and comparison with the data from crystalline references, c-BSO (**B**) and c-Bi_2O_3 (**C**).

size of the ring/void.

For our investigation, the Bi-centric D_2 PD offers the most evident insight. It is displayed in Figure 5. The PD of the RMC configuration of a-BSO (a) is best understood by comparing it with the corresponding crystalline phases as shown for c-BSO (B) and c-Bi_2O_3 (C). Their interpretation is straightforward and illustrated by the toy models in the figure: c-BSO exhibits two regions; the first at a 'birth' radius B of about 2.2 Å, which is related to the almost tetrahedral arrangement of Bi *inside* a Bi_2O_2 layer, and the second region around $B \approx 3.2 - 3.6$ Å is linked to the separation *between* the Bi_2O_2 layers. On the other hand, c-Bi_2O_3 only exhibits a single region at $B \approx 2.5$ Å with a larger lifetime (= distance from the diagonal, corresponding to the size of the void), which is related to the nearly octahedral arrangement of Bi atoms in the unit cell (see inset illustrations in Figure 5). An octahedron encompasses a larger void area than a tetrahedron, and therefore exhibits a larger lifetime in the PD. The octahedra in c-Bi_2O_3 are also slightly distorted, which leads to a distribution of data points in a limited region.

Amorphous BSO shows a mix of these characteristics: a separation into two distinct regions, with a wide-spaced first region with relatively large lifetime starting at $B \approx 2.2$ Å, and a second region above $B \approx 3.2$ Å. Owing to the nature of the amorphous phase [29], weak but long streaks towards long lifetimes are also observed, as well as a concentration of most of the signal intensity close to the diagonal line, representing the overall disordered arrangement of atoms.

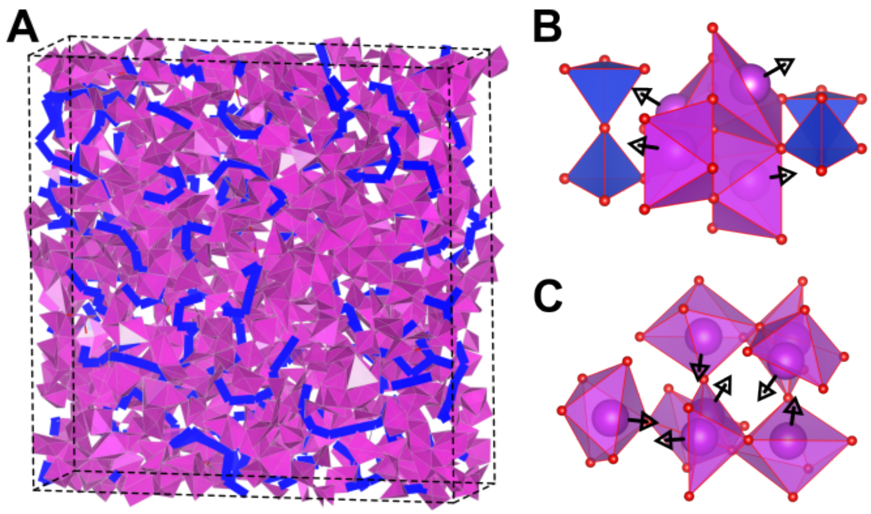

FIG. 6. (A) View of the final RMC model for a-BSO, showing a slab with a thickness of 33% of the whole simulation box. Silica chains are illustrated as blue lines, and bonding polyhedra around Bi in purple. (B) Detail of the c-BSO structure, illustrating that distortion vectors are pointed in separate regions in space, in contrast to c-Bi_2O_3 (C), in which they pairwise point into the same spatial regions.

IV. DISCUSSION

We have established that the local environment of a-BSO is made up of the same building blocks as the reference crystal phases. With this thorough analysis, we are now able to discuss the relationship between the atomic structure and the material properties of a-BSO.

The fundamental structure of a-BSO is made up of SiO_4 chains, between which a Bi_2O_3-rich phase is embedded. Note that this does *not* indicate a form of phase separation, since the Bi_2O_3-rich enclosures remain small, and there are not more than a few BiO_x clusters between each strand of the SiO_4 chains. An illustration of this architecture is given in Figure 6 A.

Together with the PD analysis, which shows characteristics both from c-Bi_2O_3 and c-BSO, these findings shed light on the 2-step crystallization behavior [8, 16] that was noted in the introduction: upon heating, at around 470 °C, initially the Bi-rich regions start to form crystallization seeds for an expanded c-Bi_2O_3 phase; subsequently, (at around 540 °C) the remaining silica phase is incorporated to form c-BSO.

Furthermore, we are also in a position to explain the large dielectric permittivity of the bismuth silicate glass. The first point to emphasize is that the experimental data on the atomic SRO proves the existence of BiO_x clusters (with predominantly x=5 and 6) in the amorphous phase, and that their local geometry resembles that of a (disordered) crystal. In other words, the O atoms are largely pushed to one side of the bond hemisphere, leading to a strongly polar atomic arrangement. This is a major driving force of the high dielectric permittivity of this material.

The IRO characteristics are another factor to increase the permittivity. Here, the connection of the SiO_4 units play a vital role: These are mainly Q^2-connected (i.e. silica chains, as they are also found in c-BSO) and, to a smaller amount, Q^3-connected. A comparable binary silicate glass is PbO-SiO_2, in which a wide distribution of Q^n values is found [35]. This is associated with a much smaller dielectric constant, e.g. ε for binary PbO-SiO_2 is only 15.5 [36] and does not surpass 24.5 for any of the known binary PbO-SiO_2 glasses [6, 37, 38].

To explain the role of the silica chains in more detail, let us consider again the structural properties of c-BSO and c-Bi_2O_3, which posses strongly different dielectric constants (90 vs. 33). The cluster polarization vectors, i.e. the vectors pointing in the direction of the displacement of Bi from the cluster centroid, are illustrated in Figure 6 B and C. These vectors essentially indicate the direction of the free electron pair of Bi. In c-BSO (B), these vectors are oriented each in a separate spatial region within the Bi_2O_2 layer. This geometry leads to a strong anisotropy of the permittivity within the Bi_2O_2 layer versus out-of-plane [16], and enables a high polarizability of each BiO_6 unit. In contrast, in c-Bi_2O_3 (C), there is no separation between the BiO_x clusters, and the Bi lone pairs are pairwise pointing into a similar spatial region. This geometry causes a frustration in the polarizability of the BiO_x clusters, and thereby reduces the permittivity of the entire system.

An analogous effect takes place in the amorphous phase (a-BSO): the nano-separation by silica chains of the Bi_2O_3-rich areas allows the displacement vectors of the BiO_x clusters to point away from each other, thus reducing the overall frustration in the cluster polarizability. Therefore, we can identify the micro-structure as another key factor to explain the materials dielectric permittivity. In particular, it provides the basis to explain why ε of a-BSO is larger than that of c-Bi_2O_3, but due to the inherent disorder it is smaller than that of c-BSO.

V. CONCLUSION

We have conducted a comprehensive investigation of the atomic structure and dielectric properties of amorphous bismuth silicate (a-BSO). By employing a combination of experimental techniques, we modeled both the short- and intermediate-range atomic structures using a Reverse Monte Carlo approach. The resulting model reveals BiO-rich regions embedded within SiO_4 chains, exhibiting notable structural similarities to the crystalline phase of Bi_2SiO_5 (c-BSO).

Amorphous bismuth silicate exhibits a much larger dielectric permittivity than any other known glass, with a value of $\varepsilon = 56$ at ambient conditions. This high dielectric permittivity is primarily attributed to the polar nature of the BiO_x polyhedra. In this configuration, oxygen atoms are largely confined to one bond hemisphere - an asymmetric arrangement that induces a significant atomic-level polarizability. In addition, the intermediate-range separation of BiO_x clusters by SiO_4 chains enables a flexibility in the local arrangements of the clusters. These two factors can be identified as the main driving forces of the material's exceptional dielectric properties.

ACKNOWLEDGMENTS

The present work was partially supported by JSPS Grants-in-Aid for Transformative Research Areas (A) "Hyper-Ordered Structures Sciences" (Grant Nos. 20H05878, 20H05879 and 20H05880) as well as the JSPS KAKENHI grants 20H02429, 20K15027 and 21K18800, and by the MEXT Program for Creation of Innovative Core Technology for Power Electronics Grant Number JPJ009777. The project was conducted as an SDGs Research Project of Shimane University.

The authors would like to thank Prof. T. Okabe in the University of Tokyo for the NMR experiments, as well as Prof. L. Pusztai of the HUN-REN Wigner Centre for Physics for stimulating discussions on the topic.

The synchrotron radiation experiments were performed at KEK-PF (Proposal Nos. 2019G133, 2021G091, and 2023G040) and at SPring-8 (Proposal no. 2021A1297). The neutron experiments at the MLF/J-PARC were performed under a long-term proposal (Proposal No. 2022L0202). The authors acknowledge Dr. T. Honda for his help in the

neutron diffraction measurement using the NOVA spectrometer at J-PARC.

[1] P. Balaya, V. K. Shrikhande, G. P. Kothiyal, and P. S. Goyal, Dielectric and conductivity studies on lead silicate glasses having mixed alkali andalkaline earth metal oxides, Current Science **86**, 553 (2004).

[2] C. H. Hsieh, H. Jain, and E. I. Kamitsos, Correlation between dielectric constant and chemical structure of sodium silicate glasses, Journal of Applied Physics **80**, 1704 (1996).

[3] M. T. Sebastian, H. Wang, and H. Jantunen, Low temperature co-fired ceramics with ultra-low sintering temperature: A review, Current Opinion in Solid State and Materials Science **20**, 151 (2016).

[4] W. H. Dumbaugh and J. C. Lapp, Heavy-metal oxide glasses, J. Am. Ceram. Soc. , 2315 (1992).

[5] M. Janewicz, J. Wasylak, and W. Bogusz, Electric properties of pbo-bi2o3-ga2o3 glasses, Materials Science and Engineering **B25**, 147 (1994).

[6] Y.-F. Chen and *et al.*, Sciglass next, https://sciglass.uni-jena.de/ (2024).

[7] J. Song, G. Zhu, H. Xu, W. Fu, J. Xu, J. Zhang, S. Huang, and A. Yu, Preparation and properties of high-density bi2o3 ceramics by cold sintering, Ceramics International **46**, 13848 (2020).

[8] H. Taniguchi, A. Kuwabara, J. Kim, Y. Kim, H. Moriwake, S. Kim, T. Hoshiyama, T. Koyama, S. Mori, M. Takata, H. Hosono, Y. Inaguma, and M. Itoh, Ferroelectricity driven by twisting of silicate tetrahedral chains, Angewandte Chemie International Edition **52**, 8088 (2013).

[9] V. Dimitrov and S. Sakka, Electronic oxide polarizability and optical basicity of simple oxides. i, Journal of Applied Physics **79**, 1736 (1996).

[10] T. Komatsu, V. Dimitrov, T. Tasheva, and T. Honma, A review: A new insight for electronic polarizability and chemical bond strength in bi2o3-based glasses, Journal of Non-Crystalline Solids **550**, 120365 (2020).

[11] T. Maeder, Review of bi2o3 based glasses for electronics and related applications, International Materials Reviews **58**, 3 (2013).

[12] B. Huang and J. Robertson, Bonding origin of optical contrast in phase-change memory materials, Physical Review B **81**, 081204 (2010).

[13] K. Shportko, S. Kremers, M. Woda, D. Lencer, J. Robertson, and M. Wuttig, Resonant bonding in crystalline phase-change materials, Nat. Mater. **7**, 653 (2008).

[14] Y. Saito, Y. Sutou, and J. Koike, Phase change characteristics in GeTe-CuTe pseudobinary alloy films, J. Phys. Chem. C **118**, 26973 (2014).

[15] J. R. Stellhorn, B. Paulus, S. Hosokawa, W.-C. Pilgrim, N. Boudet, N. Blanc, H. Ikemoto, S. Kohara, and Y. Sutou, Structure of amorphous cu2gete3 and the implications for its phase-change properties, Physical Review B **101**, 214110 (2020).

[16] H. Taniguchi, S. Tatewaki, S. Yasui, Y. Fujii, J. ichi Yamaura, and I. Terasaki, Structural variations and dielectric properties of (bi1xlax)2sio5 polycrystallines synthesized by crystallization of bi-si-o and bi-la-si-o glasses, Physical Review Materials **2**, 045603 (2018).

[17] A. Witkowska, J. Rybicki, and A. D. Cicco, Structure of partially reduced bismuth–silicate glasses: EXAFS and MD study, Journal of Alloys and Compounds **401**, 135 (2005).

[18] T. Ohkura, Y. Fujimoto, M. Nakatsuka, and S. Young-Seok, Local structures of bismuth ion in bismuth-doped silica glasses analyzed using bi lsubIII/subx-ray absorption fine structure, Journal of the American Ceramic Society **90**, 3596 (2007).

[19] M. Todea, R. Turcu, M. Vasilescu, D. Trandafir, and S. Simon, Structural characterization of heavy metal SiO2–bi2o3 glasses and glass–ceramics, Journal of Non-Crystalline Solids **432**, 271 (2016).

[20] F. Miyaji and S. Sakka, Structure of pbo-bi2o3-ga2o3 glasses, Journal of Non-Crystalline Solids **134**, 77 (1991).

[21] A. Masuno, Structure of densely packed oxide glasses prepared using a levitation technique, Journal of the Physical Society of Japan **91**, 10.7566/jpsj.91.091003 (2022).

[22] W. Gu, F. Teng, Z. Liu, Z. Liu, J. Yang, and Y. Teng, Synthesis and photocatalytic properties of bi2sio5 and bi12sio20, Journal of Photochemistry and Photobiology A: Chemistry **353**, 395 (2018).

[23] O. Gereben, P. Jóvári, L. Temleitner, and L. Pusztai, A new version of the RMC++ reverse monte carlo programme, aimed at investigating the structure of covalent glasses, J. Optoelectron. Adv. Mater. **9**, 3021 (2007).

[24] O. Gereben and L. Pusztai, RMC_POT: A computer code for reverse monte carlo modeling the structure of disordered systems containing molecules of arbitrary complexity, J. Comput. Chem. **33**, 2285 (2012).

[25] I. Obayashi, T. Nakamura, and Y. Hiraoka, Persistent homology analysis for materials research and persistent homology software: HomCloud, Journal of the Physical Society of Japan **91**, 091013 (2022).

[26] H. Edelsbrunner and J. Harer, *Computational Topology: An Introduction* (Am. Mathematical Soc., Providence, RI, 2010).

[27] Y. Hiraoka, T. Nakamura, A. Hirata, E. G. Escolar, K. Matsue, , and Y. Nishiura, Hierarchical structures of amorphous solids characterized by persistent homology, Proc. Natl. Acad. Sci. USA **113**, 7035 (2016).

[28] M. Murakami, S. Kohara, N. Kitamura, J. Akola, H. Inoue, A. Hirata, Y. Hiraoka, Y. Onodera, I. Obayashi, J. Kalikka, N. Hirao, T. Musso, A. S. Foster, Y. Idemoto, O. Sakata, and Y. Ohishi, Ultrahigh-pressure form of sio2 glass with dense pyrite-type crystalline homology, Phys. Rev. B **99**, 045153 (2019).

[29] Y. Onodera, S. Kohara, S. Tahara, A. Masuno, H. Inoue, M. Shiga, A. Hirata, K. Tsuchiya, Y. Hiraoka, I. Obayashi, K. Ohara, A. Mizuno, and O. Sakata, Understanding diffraction patterns of glassy, liquid and amorphous materials via persistent homology analyses, J. Ceram. Soc. Jpn. **127**, 853 (2019).

[30] P. J. Steinhardt, D. R. Nelson, and M. Ronchetti, Bond-orientational order in liquids and glasses, Physical Review B **28**, 784 (1983).

[31] A. Baranyai, A. Geiger, P. R. Gartrell-Mills, K. Heinzinger, R. McGreevy, G. Pálinkás, and I. Ruff, Invariants of spherical harmonics as order parameters in liquids, J. Chem. Soc., Faraday Trans. 2 **83**, 1335 (1987).

[32] M. J. Cliffe and A. L. Goodwin, Quantification of local geometry and local symmetry in models of disordered materials, physica status solidi (b) **250**, 949 (2012).

[33] T. Ohkubo, A. Masuno, E. Tsuchida, and S. Ohki, Theoretical insights into the 27al nmr parameters of binary aluminosilicate glass and their relationship to the atomic and electronic structure, The Journal of Physical Chemistry C 10.1021/acs.jpcc.3c06292 (2024).

[34] T. Ohkubo, S. Sasaki, A. Masuno, and E. Tsuchida, Ab initio molecular dynamics study of trivalent rare earth rich borate glasses: Structural insights and formation mechanisms, The Journal of Physical Chemistry B **128**, 11800 (2024).

[35] S. Kohara, H. Ohno, M. Takata, T. Usuki, H. Morita, K. Suzuya, J. Akola, and L. Pusztai, Lead silicate glasses: Binary network-former glasses with large amounts of free volume,

Physical Review B **82**, 134209 (2010).

[36] H. Hagiwara and R. Oyamada, Dielectric constant, infrared absorption and raman effect of glassy fe2o3-pbo-sio2 system, Journal of the Ceramic Association Japan **84**, 264 (1976).

[37] Y. Wang, M. Kobayashi, A. Osaka, Y. Miura, and K. Takahashi, Anionic conduction in lead halosilicate glasses, Journal of the American Ceramic Society **71**, 864 (1988).

[38] A. Osaka, Y.-h. Wang, M. Kobayashi, Y. Miura, and K. Takahashi, Packing of atoms in lead halosilicate glasses of low silica content, Journal of Non-Crystalline Solids **105**, 63 (1988).